Theoretical and Experimental Analysis of the Directional RI Sensing Property of Tilted Fiber Grating

Yuezhen Sun, Tean Lu, Yarien Moreno, Liangye Li, Hushan Wang, Kaiming Zhou, Qizhen Sun, Deming Liu, Zhijun Yan and Lin Zhang

Abstract— In this paper, we have theoretically and experimentally investigated the unique vector refractive index (RI) sensing property of tilted fiber grating (TFG). Due to the orthogonal symmetric grating structure, TFGs would mainly achieve the coupling between the fiber core mode and the two orthogonal polarization LP_{1m} of cladding mode. And the numerical simulation results showed that the coupling coefficient between fundamental core mode to the LP_{1m} cladding mode is higher than the others. In the experiment, we have furthermore observed the cladding mode field distribution of excessively TFG (Ex-TFG) and long period fiber grating (LPFG), which indicated that the evanescent field distribution of cladding mode of TFG shows an asymmetric near field distribution with two lobes oriented along the fast axis of TFG, and the one of LPFG has a circularly symmetric cladding mode field distribution. In addition, by employing side-immersion method, we have measured the azimuth RI sensitivities of Ex-TFG, tilted fiber Bragg grating (TFBG) and LPFG, which exhibited that both Ex-TFG and TFBG have shown a direction-dependency RI sensitivity, and the RI sensitivity with side-immersion along fast axis is almost half of the one along slow axis, and the RI sensitivity of LPFG is azimuth independent. Overall, the experiment results show that the TFGs inherently show unique directional RI sensing property, which could be potentially applied in vector sensing area.

Index Terms—Coupled mode analysis, Fiber gratings, Optical sensors, Vector measurement.

I. Introduction

Vector monitoring is an essential technology in many branches of mechanical measurement and electromagnetic detection, such as aerospace, geologic examination, mineral exploitation and power transmission [1-6]. Both direction information and amplitude information are the key points to precisely identify the physical quantities in practical measurement. Traditional vector measurements generally require multiple measurements in different directions and vector synthesis, which are cumbersome to operate and complex in structure. For various application field, fiber optic sensors are well suitable for vector monitoring due to their merits of compact size, high sensitivity, immunity to electromagnetic interference and easy integration. The common methods, to realize the vector measurement in two dimensions or three dimensions, are involving asymmetrical structure, such as separated fibers or fiber gratings through eccentric fusion splicing, polishing or corroding the surface of fibers, combining several fiber sensors. Mao et al. fabricated fiber Bragg gratings (FBGs) in a hollow eccentric fiber which is suitable for distinguishing bending direction [7]. Ou et al. demonstrated a bending vector sensor fabricated by splicing the seven-core photonic crystal fiber (PCF) to single mode fiber with a lateral offset splicing point to form a Mach-Zehnder interferometer (MZI) [8]. Jiang et al. reported a high sensitivity directional torsion sensor based on the chiral long period fiber grating (LPFG) inscribed in the twisted double-cladding fiber by CO_2-laser [9]. Jiang et al. presented a ferrofluid integrated side-polished-fiber-based magnetic field sensor with sensitivity enhancement using surface plasmon resonance (SPR) [10]. Francesco Chiavaioli et al. proposed a device based on a pair of identical LPFGs, a microresonator and the tapered fiber in between, which could excite novel modes [11]. Therefore, only simple symmetric fiber structures or fiber gratings (FBG or LPFG) are unfeasible, and the non-circular-symmetrical structure must be employed in all above proposed configurations and is the key to achieve vector sensing, in other words, the asymmetric evanescent field of the fiber grating results in vector sensing in essence. However, these sensors require complex processing which are bad for repetitive verification and difficult for practical production and application. Thus, the present issue is how to use a single fiber sensor or device to meet requirements of vector measurement.

Different from the normal fiber gratings (FBGs or LPFGs), tilted fiber gratings (TFGs), such as TFBGs and Ex-TFGs, have an internal asymmetric structure, and their grating planes are

Y. Sun, T. Lu, Y. Moreno, L. Li, Q. Sun, Z. Yan, and D. Liu are with the School of Optical and Electronic Information, Huazhong University of Science and Technology, Wuhan 430074, China.

Q. Sun, Z. Yan, and D. Liu are with the Wuhan National Laboratory for optoelectronics, Huazhong University of Science and Technology, Wuhan 430074, China.

K. Zhou and L. Zhang are with the Aston Institute of Photonic Technologies, Aston University, Birmingham B4 7ET, U.K.

H. Wang is with the State Key Laboratory of Transient Optics and Photonics, Chinese Academy of Sciences, Xi'an Institute of Optics and Precision Mechanics, Xi'an 710119, China.

blazed pattern with respect to the normal of optical fiber axis, which could be potentially applied for vector sensing. The TFBG was firstly reported by G. Meltz in 1990 [12], which has a short grating period and slightly tilted grating pattern with respect to optical fiber axis, resulting in a Bragg resonance peak and hundreds of polarization dependent cladding modes. So far, researchers have proposed many different configurations based on TFBG to achieve vector measurements including vector vibroscope [13], vector rotation sensor [14], vector magnetometer [15] and so on. In 2006, Zhou et al. has reported a fiber grating with >80° tilted structures [16], which were renamed as Ex-TFG in later research as their grating planes are excessively tilted and there is not the Bragg reflection peak in its transmission spectrum. The Ex-TFGs have longer grating periods and larger tilted angles than TFBGs, which could couple the core mode into forward propagation cladding mode and there is a series of dual-peak resonances corresponding to two sets of polarization dependent modes (TM/TE) in the transmission spectrum. In 2016, Yan et al. have theoretically and experimentally investigated the dual-peak feature of Ex-TFG and its temperature and RI sensitivity characteristics [17-18], and the polarization-related coupling property has promoted Ex-TFGs to be applied as twisting [19] and transverse loading sensors [20]. In our previous work [21], we proposed and demonstrated a compact vector magnetometer based on the Ex-TFG assistant with magnetic fluid. However, there are not any papers to systematically explain the mechanism of how TFGs could be used for vector sensing. In this paper, we have investigated and unveiled the directional RI sensing property of the TFG. The mode coupling behavior of TFGs has been discussed and simulated, and the cladding mode near field profile of Ex-TFG has been observed. In addition, we have designed and experimentally investigated the direction-dependency of RI sensitivity of TFGs by using side-immersion method. By comparing with the performance of LPFG, we could conclude that the TFGs have inherent and specific characteristic of direction-dependent RI sensitivity and could be potentially applied in the vector measurement.

II. Mode Characteristics And Fabrication

A. Mode Couplings in Fiber Grating

The LPFG with a symmetrical refractive index modulation in fiber core could generate the mode couplings between the core mode and the cladding modes. According to the theoretical analysis in Ref. [22], The LPFG can only excite cladding modes with azimuthal order $\mu = 1$ which is concluded from the azimuthal integral in coupling coefficient:

$$\int_0^{2\pi} d\phi \exp[i(\mu - 1)\phi] = 2\pi\delta_{\mu 1} \qquad (1)$$

where μ is the azimuthal order, and $\delta_{\mu 1}$ is the Kronecker delta function, which is equal to 1 only when $\mu = 1$. In weakly guiding (LP) approximation, it is equivalent to that the LP_{01} core mode only couples to the LP_{0m} cladding modes for LPFG. However, the coupling behaviors in the TFGs are more complicated. Due to the tilt angle of the grating, the interaction would occur between the core mode and higher order cladding

modes with any azimuthal order. Considering the tilt angle θ in TFG, the coupling coefficient components between a LP_{01} core mode and hybrid (lm) mode can be expressed as [23]:

$$g_{lm-01}^{cl} = A_g^{cl} \int_0^a rdr J_{l-1}(2rK_g sin\theta)$$
$$\times J_{l-1}(u_{lm}r)J_0(u_0 r) \quad (2)$$

where A_g^{cl} is the amplitude of the cladding mode, a is the core radius, J is the Bessel function of the first kind, K_g is the wave number of TFG, $u_{lm}^2 \equiv (2\pi/\lambda)^2(n_1^2 - n_{efflm}^2)$ (n_1 and n_{efflm} are the refractive index of core material and effective index of cladding mode, respectively), θ is the tilt angle of the grating.
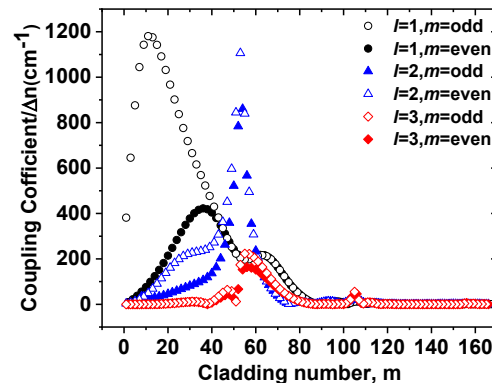

Fig. 1. Coupling coefficients for cladding modes with l=1,2,3 in a tilted fiber grating

It is reported that the TFGs could achieve the cladding mode couplings for l>0, and the simulation analysis has shown that the mode coupling coefficients between cladding modes with azimuthal mode number l=1,2,3 and core mode is 10 times higher than the one of cladding mode with l>3 [23-26]. The coupling coefficients g_{lm-01}^{cl} that describe the mode coupling between an LP_{01} core mode and hybrid (lm) cladding modes of l=1,2,3 are plotted in Fig.1. As shown in the figure, cladding mode coupling in TFG mainly occurs at the first 40 orders when l=1, and mainly occurs at 40~60th order or 50~70th order for l=2 or 3, respectively. According to the simulation results, we find that cladding number of the main coupling range would move high order while azimuthal mode number l increases. Actually, in our experiment, the axial period of Ex-TFG is around tens micrometer and the one of TFBG is sub-micrometer, in which the mode coupling mainly happens between core mode and the first 40 orders cladding mode. So, we mainly observe mode coupling of TFGs that LP_{01} core mode mainly couples to the LP_{1m} cladding modes, and the mode couplings between the LP_{01} core mode and the higher order cladding modes are at least an order of magnitude smaller than those with LP_{1m} cladding modes in TFGs.

B. Cladding Mode Field Distributions

Due to the tilted grating plane, TFGs could couple forward propagating core mode into polarization dependent forward/backward propagating cladding modes. So far, TFGs have been reported as various biochemical sensors [27-33] and physical sensors [19-21, 34-35]. The relationship between resonance wavelength of cladding modes and surrounding refractive index (SRI) could be determined by phase match

condition (PMC) of TFGs:

$$\lambda_{res} = \left(n_{eff}^{co} \pm n_{eff}^{cl,m}(n_{SRI}) \right) \frac{\Lambda_G}{cos\theta} \qquad (3)$$

Where, λ_{res} is the resonance wavelength; n_{eff}^{co} is the effective index of core mode, which is not directly affected by surrounding perturbation; $n_{eff}^{cl,m}$ is the effective index of mth cladding mode; n_{SRI} is the SRI; Λ_G is the normal period of grating; θ is the tilted angle of the grating, and the "+" and "-" correspond to backward coupling behavior (TFBGs) and forward coupling behavior (Ex-TFGs), respectively.
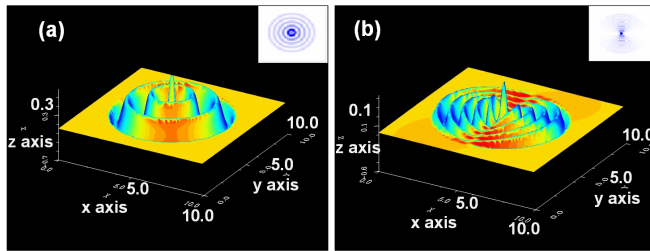

Fig. 2. Simulation results of cladding mode distribution of (a) LP_{06} mode and (b) $LP_{1,10}$ mode.

The nature of RI sensing of fiber grating is that the effective refractive index of cladding mode is affected by SRI, furthermore, the evanescent field of cladding mode interacts with surrounding mediums [18, 36]. On the other hand, only the changing of RI within evanescent field of cladding mode would affect the cladding mode index. Therefore, the evanescent field distribution of cladding mode would determine the RI sensitivity. As analyzed in the previous section, the LPFG only excites the coupling behaviors between LP_{01} core mode and LP_{0m} cladding modes, and the TFG, due to asymmetric structure, mainly couples the core mode into non-circularly (LP_{1m}) symmetric propagating cladding modes. Using Optigrating (from Optiwave), we have simulated the cladding mode field distribution of $LP_{0,6}$ and $LP_{1,10}$, which are depicted in Fig.2a and 2b, respectively. As it is shown in the figure, the $LP_{0,6}$ has a circularly symmetrical mode field distribution, and $LP_{1,10}$ has an azimuthally asymmetrical mode field distribution. And the fiber grating axis is the z axis shown in the figure. In detail, the evanescent field is concentrated on the x axis, which signifies that when the TFG is disturbed by the external environment, the overlap between evanescent field of cladding mode and outer medium would be stronger on x axis than y axis. Furthermore, when the main transmission modes in the fiber are LP_{lm} ($l>1$) modes, its evanescent field distribution is circularly symmetric, which leads to a more even distribution.

Generally speaking, the change of effective index of cladding modes resulting from surrounding perturbation is the key factor to determine the resonance wavelength. Essentially, wavelength shift relies on penetration of the evanescent field of the cladding modes into the outer medium [37]. The evanescent field of the cladding mode overlaps more maximally with the penetration of surrounding environment, which will induce the largest wavelength shift. Thus, for the LPFG and other fiber gratings with the main transmitted cladding modes of LP_{lm} ($l>1$) due to its symmetrical grating structure, it will have a uniform azimuth RI, but for TFGs, the response to RI of fiber gratings on x axis would be more sensitive than y axis, which could make the TFG has direction dependent sensitivity.

Consequently, only the LP_{1m} cladding mode of fiber grating could show vector RI sensing characteristics because of its uneven evanescent field distribution.

C. Fiber Grating Fabrication and Spectra

In this paper, three different fiber gratings are fabricated and investigated, including Ex-TFG, TFBG and LPFG, which are UV-inscribed by using amplitude mask scanning method, phase mask scanning method and point by point method respectively. During the fabrication process of Ex-TFG, we used a custom-
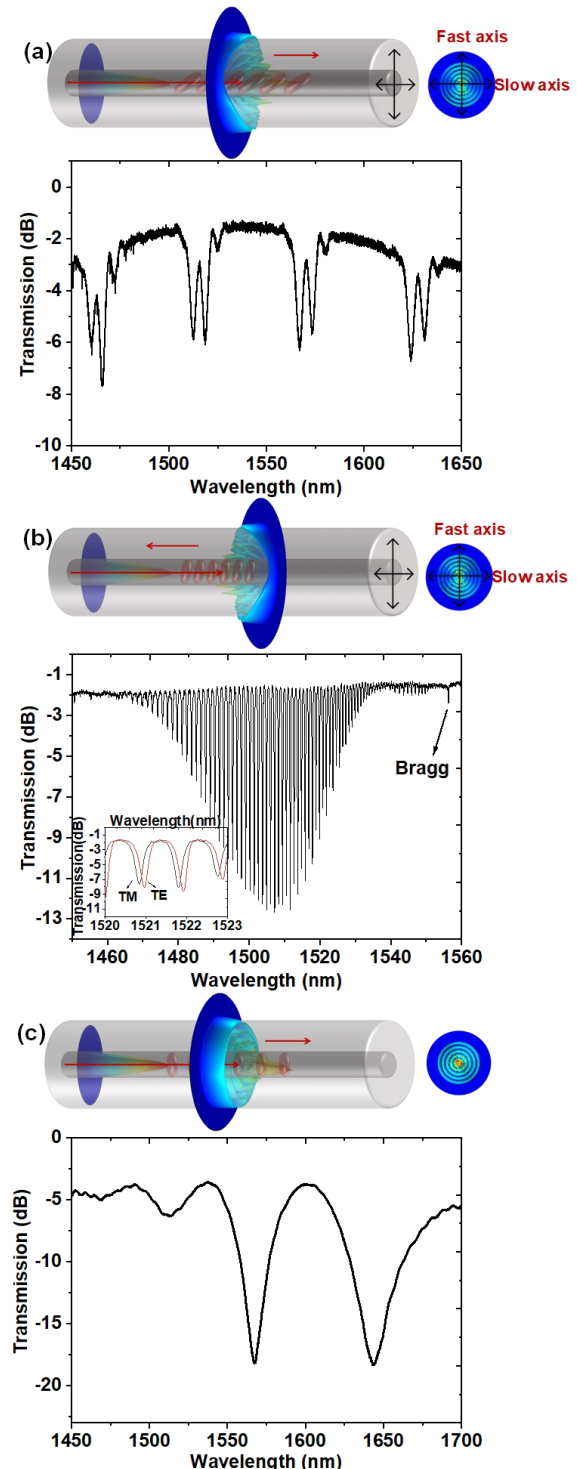

Fig. 3. Grating structures and Transmission spectra of the (a) Ex-TFG, (b) TFBG and (c) LPFG.

designed amplitude mask with a period of 5μm, that was tilted at angle of 80° with respect to the normal of fiber axis to generate a 28.8μm axial grating period. As for TFBG used in this work, we utilized ±1 order diffraction of phase mask with 1068 nm period tilted at 7.5° to fabricate a 10° TFBG. For comparison, a LPFG with a period of 160μm was fabricated by point-by-point inscription method.

The grating structure and transmission spectrum of Ex-TFG, TFBG and LPFG are depicted in Fig. 3a-c, in which the Ex-TFG has a series of dual-peak polarization dependent cladding mode resonance; the TFBG has comb-like polarization dependent cladding mode resonance peaks and LPFG has several separated resonance cladding mode peaks. The detailed spectral characterization of Ex-TFG, TFBG and LPFG have been reported in [17,38].

D.   Near Field Distribution Profiles

To verify the simulation results, we have experimentally observed the cladding modes near field distribution of LPFG and Ex-TFG (we can't directly measure cladding mode distribution of TFBG, due to its backward propagation property), respectively [35]. The experimental setup is shown in Fig. 4, which consists of a tunable laser, a polarization controller (PC), a fiber rotator, an objective lens and a beam profiling camera (Gentec-EO Beamage-4M-IR). During the experiment, the wavelength of the tunable laser is set to be the resonance wavelength of cladding mode (1535 nm for LPFG, 1565 nm for Ex-TFG). The PC is used to control the polarization state of light launched into Ex-TFG. By employing fiber rotator, we can clamp and adjust the azimuth of the fiber grating with an accuracy of 1° to control the relative direction.
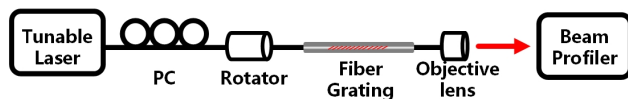

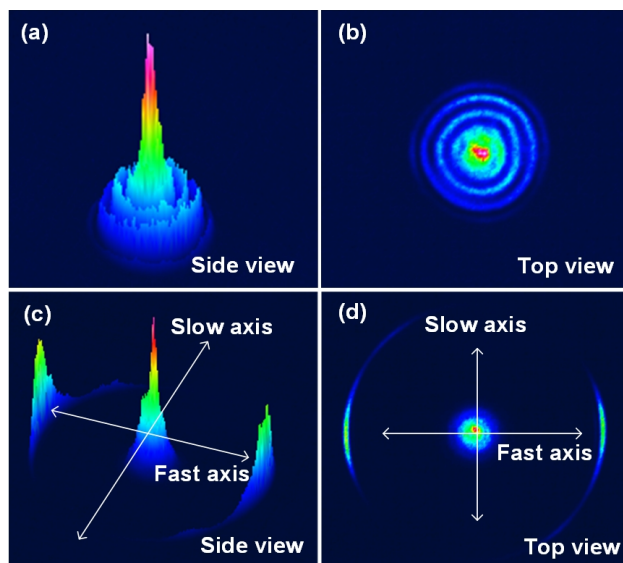Fig. 4.   Experimental setup for capturing the cladding mode field distribution.

Fig.5. Captured near field distribution patterns of (a) (b) the LPFG and (c) (d) the Ex-TFG, respectively.

With proper polarization state and fiber position calibration, the clear near field distribution patterns of LPFG and Ex-TFG

could be captured by beam profiling camera and are shown in Fig. 5. As it shown in the figure, the LPFG has circular-symmetrical field distribution, and the cladding mode near field distribution of the Ex-TFG mostly has two lobes oriented along the direction of fast axis, which are agree well with the simulation results.

III.   EXPERIMENTAL RESULTS AND DISCUSSIONS

A.   Side-immersion RI measurement methods

To measure and evaluate the RI response at different azimuths of TFGs and LPFG, we have designed a side-immersion method. The experimental setup is shown in Fig. 6, which consists of a broadband light source (BBS), a polarizer, a polarization controller (PC), two fiber rotators with a resolution of 2°, a translation stage and an optical spectrum analyzer (OSA) with a resolution of 20 pm. The polarizer and the PC are used to generate and control the polarization state of light launched into the TFG. As we discussed in previous section that the overlap between evanescent field and surroundings determine if the fiber sensor has the RI response, by contacting partial fiber cladding with RI medium, see the inset of Fig. 6, we could evaluate that the fiber sensors has directional RI response.
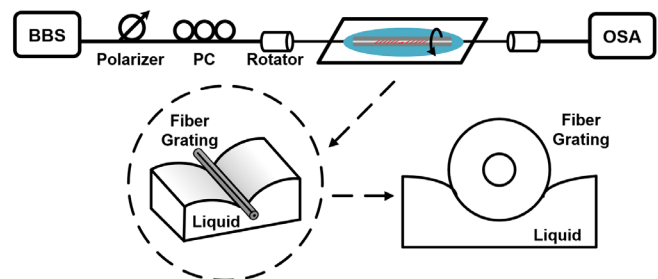

Fig. 6.   Experimental setup for measuring the azimuth RI sensitivity with sidely immersion into liquid.

The experimental procedures for measuring the RI response at different azimuth of fiber grating are listed as following: (1). The RI oil is placed on the translation stage, which could be controlled to ensure that liquid would immerse the fiber cladding gradually by raising stage. Due to the surface tension, during raising up the stage, the fiber is not entirely immersed into RI oil, but stands on the surface of RI oil due to the surface stress. Then, the transmission spectrum is recorded. (2). Before measuring RI response at next azimuth, the surface of fiber is cleaned by pure ethanol until the original spectrum in air is restored in the OSA. Then the grating is rotated with 15° and repeating the first step. It is worth noting that the effect of twist on the light polarization launched into the TFG must be eliminated by adjusting the PC to restore the spectrum. (3) The spectrum evolution of RI response is measured through rotating the fiber grating from 0° to 360° with a 15° increment.

B.   RI Response Results of Different Fiber Gratings

In this section, we would measure the RI response with different immersion angle of three different fiber gratings: (1) Ex-TFG with a tilted angle of 80°; (2) TFBG with a tilted angle of 10°; (3) LPFG with a period of 160μm. The fast/slow axis of

the TFG has been marked before the grating inscription.

1) RI Response of the Ex-TFG

TE and TM cladding mode of Ex-TFG are a pair of degenerate mode, which have the same RI sensing performance [17]. In our experiment, we only evaluate the TM cladding mode. And the RI used is around 1.39 to make sure the peak separated totally. In the first place, we have explored the RI response from the fast axis staying horizontal, which marked as 0°, and when the angle is turned to 90°, the detection direction is the slow axis.

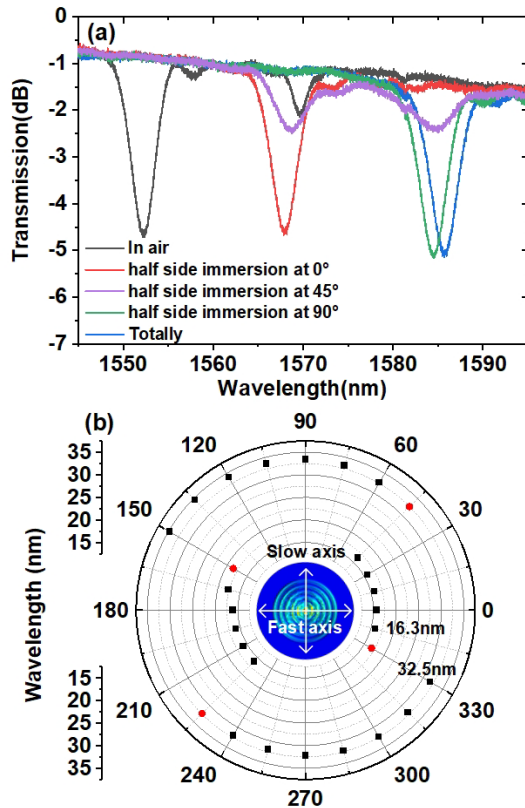Fig. 7. Transmission spectra response of TM mode of Ex-TFG by sidely immersing 1.39 RI oil (a) along 0°, 45°, 90° and fully; (b) along different immersion angles with respect to the fast axis of grating from 0° to 345° in polar coordinates

According to the measuring method described in the previous section, we have recorded the transmission spectrum response of TM mode of Ex-TFG at different azimuth, which is shown in Fig. 7. As it shown in Fig. 7, we can clearly see that the wavelength shift along slow axis (with 90°) moves similarly to the entirely immersing, which is around twice than the one along fast axis (with respect to 0°). And there is an intermediate state (at the angle of 45°, 150°, 225° and 330°) that the transmission spectra exists two peaks with equal transmission intensity (in Fig. 7a), which corresponds to the red circular dot and black cubic dot in Fig. 7b. While rotating the fiber grating from 0° to 345°, the resonance wavelength shift is about 16.3nm around fast axis and 32.5nm around slow axis in polar coordinates. The results are in good consistent with the aforementioned mode field distribution analysis, which can mutually verify that smaller wavelength shift happens in the state when half power of the evanescent field permeates

surrounded by RI oil, and the larger wavelength shift corresponds to the interaction of the whole power. The transitional spectrum evolution is caused by the asymmetric perturbation of power distribution in two lobes at the other angles.
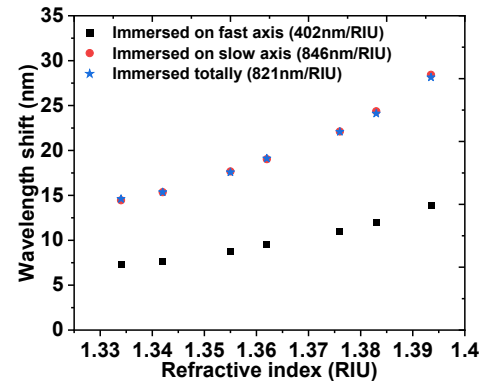

Fig. 8. RI response of Ex-TFG by sidely immersing along the fast/slow axis and fully immersing.

Besides, the RI sensitivities of side-immersion oriented along fast/slow axis of Ex-TFG are also measured, the results of which are shown in Fig. 8. In the experiment, the relative direction of Ex-TFG remains unchanged, and the RI increases from 1.33 to 1.39. Same as above results, when the Ex-TFG is sidely immersed oriented along slow axis, the wavelength shift is always larger than that of the one along the fast axis in different RI oil. In addition, the RI response of slow axis is similar with the one fully immersed, and they both have higher RI sensitivity (846 nm/RIU along slow axis immersed and 821 nm/RIU under fully immersed) than fast axis (402 nm/RIU). Being immersed oriented along slow axis can get the approximative result like entirely immersion, which also laterally indicated that the power distribution of Ex-TFGs have asymmetric, polar and concentrated profiles gathered at the direction of fast axis to interact with surrounding environment.

2) RI Response of the TFBG

Moreover, different from the Ex-TFG, TFBG has backward coupling behavior, but also possesses the tilted structure. To check these special characteristics whether be applicable for TFBG, the azimuth RI response at the direction of fast/slow axis under the RI value of 1.38 are measured with the same steps. Here, high RI oil of 1.38 is chosen for obtaining clear phenomenon of spectrum change due to the dense distribution of cladding modes and the relative low RI sensitivity of bare TFBG. Fig. 9a and b have shown the transmission spectra of several cladding modes while one-side immersion. It can be clearly observed that the response is similar with Ex-TFG. The spectrum when TFBG is immersed at the direction of slow axis, coincides with the one when TFBG is fully immersed. And the condition of fast axis induces a shorter red-shift than fully immersion. Meanwhile, the RI sensitivities of side-immersion along the fast/slow axis are measured, the results are similar with that of Ex-TFG. As shown in Fig.9c, the RI response of slow axis and fully immersed are the same around 9nm/RIU, which is twice than detecting on fast axis (4.67nm/RIU).
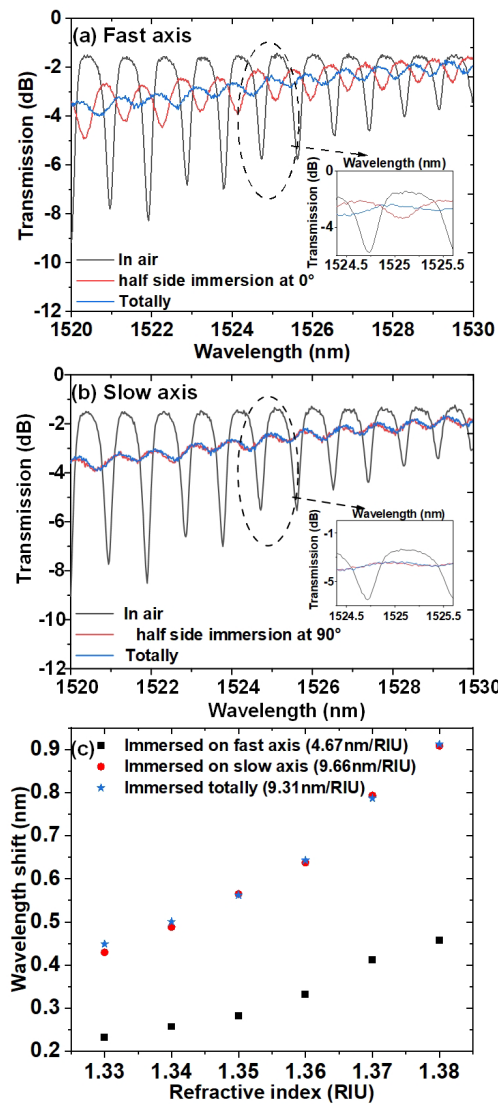
Fig. 9. Transmission spectra response of TM mode of TFBG by sidely immersing into 1.38 RI oil along (a) the fast axis and (b) the slow axis; (c) RI reponse of TFBG when immersing sidely along the fast/slow axis and immersing fully.

3) RI Response of LPFG

For a comparison, the RI response of the LPFG which possesses symmetric evanescent field is also evaluated in same condition. The blue line in Fig. 10 shows the wavelength shift of cladding mode when we entirely immersed LPFG into RI oil value of 1.411, in which the resonance peak around 1562 nm would have a blue shift of 42.58 nm with increasing RI from 1 to 1.411. Then we followed the same procedures above to one-side immerse the LPFG into RI oil, and then measured the azimuth RI sensitivity by rotating the LPFG from 0° to 345° with a 15° increment in a constant RI oil (n=1.411). Fig. 10 shows that the resonance peak is likewise blueshift to shorter wavelength, but has smaller wavelength shift (around 25 nm) among all angles than that one fully immersed, which has indicated that the transmission response of sidely immersing LPFG didn't depend on the immersing angle, due to its circular-symmetrical field distribution. And the RI sensitivities are also recorded shown in Fig.10c, in which can be seen that the RI

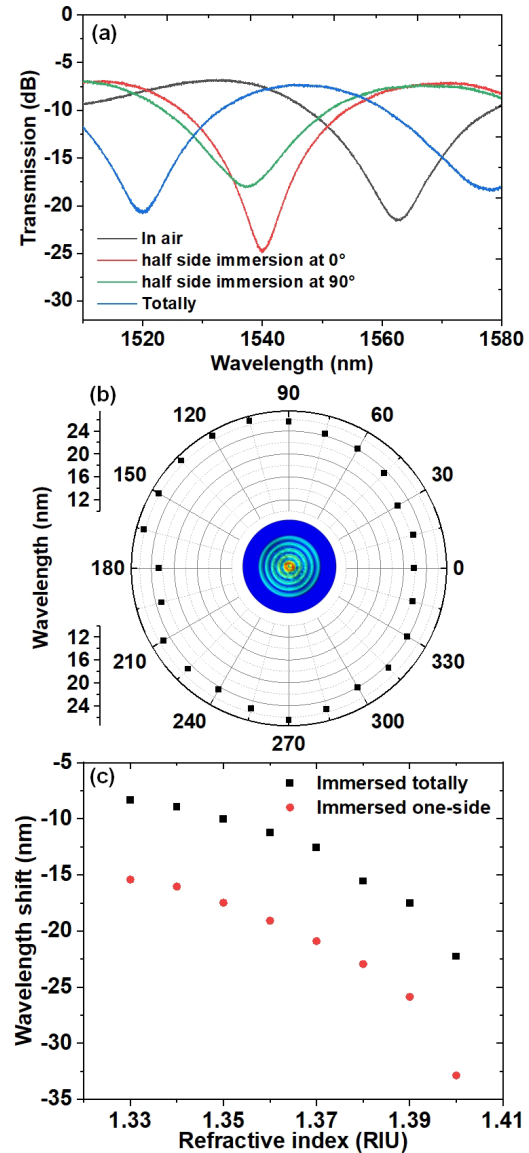sensitivity of immersed fully is almost twice than that of sidely immersed.

Fig. 10. Transmission spectra response and wavelength shifts of LPFG by sidely immersing 1.41 RI oil (a) along 0°, 90° and fully; (b) along different immersion angles from 0° to 345° in polar coordinates;(c) RI reponse of LPFG by sidely and fully immersing into different RI.

According to the above analysis, the evanescent field of the LPFG is circular-symmetric, so that the wavelength shifts of cladding mode along all azimuths are relatively small and similar when the partial medium change from air to liquid. However, there are also some minor deviations in wavelength position and amplitude among all azimuths. These reasons might result in these discrepancies: (1) during the LPFG photo-inscription process, photo-induced birefringence is caused by that only one side of fiber is always exposed to the UV laser, resulting in non-uniformity of refractive index profile in the fiber cross-section; (2) mechanical error of rotators causes the twist or non-horizontal in the LPFG during rotating; (3) there is minor difference of immersion extent every time, resulting in the uncertain penetration by varying degrees. Overall, different from the TFG, the LPFG exhibits the uniform RI sensitivity among all azimuths.

IV. CONCLUSION

In conclusion, we have investigated the directional RI response property of the TFGs, which could be potentially applied in vector sensing area. Due to the orthogonally symmetric grating structure, the TFG could couple the core mode into the LP_{1m} of cladding mode, which shows a rhombically symmetric cladding mode field distribution. Such non-circular symmetric cladding mode field distribution induces directional RI response. In the experiment, we have tested the azimuth RI sensitivities for three different fiber gratings (Ex-TFG, TFBG, LPFG) by using sidely immersing method, in which the fiber grating area is touched with the surface of RI oil duo to the surface stress. The results show that both Ex-TFG and TFBG have direction-dependency RI sensitivity, because of their asymmetric evanescence field distribution, especially, the RI sensitivity along slow axis of grating structure is the higher than the one along fast axis. We also compare the experiment of the LPFG. unlike TFGs, the LPFG has the uniform RI sensitivity among all azimuths. Overall, the TFGs showed a directional RI sensing property, which could potentially apply in the field of military, industry, national defense, and so on.

REFERENCES

[1] P. Saffari et al., "Long period grating in multicore optical fiber: an ultra-sensitive vector bending sensor for low curvatures," Opt. Lett., vol. 39, no. 12, pp. 3508-3511, 2014.

[2] T. Guo, F. Liu, F. Du, Z. Zhang, C. Li, B. Guan, and J. Albert, "VCSEL-powered and polarization-maintaining fiber-optic grating vector rotation sensor," Opt. Exp., vol. 21, no. 16, pp. 19097-19102, 2013.

[3] V. Annovazzi-Lodi, S. Donati, and S. Merlo, "Coiled-fiber sensor for vectorial measurement of magnetic field," J. Lightwave Technol., vol. 10, no. 12, pp. 2006-2010, 1992.

[4] A. Hilgers, H. de Feraudy, and D. Le Quéau, "Measurement of the direction of the auroral kilometric radiation electric field inside the sources with the Viking satellite," J. Geophys. Res-Space Phys., vol. 97, no. A6, pp. 8381-8390, 1992.

[5] R. S. Nerem, C. Jekeli, and W. M. Kaula, "Gravity field determination and characteristics: Retrospective and prospective," J. Geophys. Res.-Atmos., vol. 100, no. B8, pp. 15053-15074, 1995.

[6] Y. I. Wu et al., "The Acoustic Vector-Sensor's Near-Field Array-Manifold," IEEE Trans. Signal Process., vol. 58, no. 7, pp. 3946-3941, 2010.

[7] G. Mao et al., "Fiber Bragg grating sensors in hollow singleand two-core eccentric fibers," Opt. Exp., vol. 25, no. 1, pp. 144-150, 2017.

[8] Z. Ou et al., "Ambient refractive index-independent bending vector sensor based on seven-core photonic crystal fiber using lateral offset splicing," Opt. Exp., vol. 21, no. 20, pp. 23812-23821, 2013.

[9] C. Jiang, Y. Liu, L. Huang, and C. Mou, "Double Cladding Fiber Chiral Long-Period Grating-Based Directional Torsion Sensor," IEEE Photon. Technol. Lett., vol. 31, no. 18, pp. 1522-1525, 2019.

[10] Z. Jiang et al., "High-sensitivity vector magnetic field sensor based on side-polished fiber plasmon and ferrofluid," Opt. Lett., vol. 43, no. 19, pp. 4743-4746, 2018.

[11] Chiavaioli, F.; Laneve, D. et al. "Long Period Grating-Based Fiber Coupling to WGM Microresonators," Micromachines., vol. 9 (7), no. 366, 2018.

[12] G. Meltz, W. W. Morey, and W. H. Glenn, "In-fiber Bragg grating tap," in Proc. Opt. Fiber Commun. Conf., San Francisco, CA, USA, 1990, Paper TUG1.

[13] T. Guo, L. Shang, Y. Ran, B. Guan, and J. Albert, "Fiber-optic vector vibroscope," Opt. Lett., vol. 37, no. 13, pp. 2703-2705, 2012.

[14] T. Guo, F. Liu, B. Guan, and J. Albert, "Polarimetric multi-mode tilted fiber grating sensors," Opt. Exp., vol. 22, no. 6, pp. 7330-7336, 2014.

[15] Z. Zhang et al., "Plasmonic fiber-optic vector magnetometer," Appl. Phys. Lett., vol. 108, no. 10, pp. 101105-101108, 2016.

[16] K. Zhou, L. Zhang, X. Chen, and I. Bennion, "Optic sensors of high refractive-index responsivity and low thermal cross sensitivity that use fiber Bragg gratings of >80 ° tilted structures," Opt. Lett., vol. 31, no. 9, pp. 1193-1195, 2006.

[17] Z. Yan et al., "Theoretical and experimental analysis of excessively tilted fiber gratings," Opt. Exp., vol. 24, no. 11, pp. 12107-12115, 2016.

[18] Z. Yan et al., "Refractive index and temperature sensitivity characterization of excessively tilted fiber grating," Opt. Exp., vol. 25, no. 4, pp. 3336-3346, 2017.

[19] X. Chen, K. Zhou, L. Zhang, and I. Bennion, "In-Fiber Twist Sensor Based on a Fiber Bragg Grating With 81° Tilted Structure," IEEE Photon. Technol. Lett., vol. 18, no. 24, pp. 2596-2598, 2006.

[20] R. Suo, X. Chen, K. Zhou, L. Zhang, and I. Bennion, "In-fibre directional transverse loading sensor based on excessively tilted fibre Bragg gratings," Meas. Sci. Technol., vol. 20, no. 3, pp. 034015, 2009.

[21] T. Lu et al., "Excessively tilted fiber grating-based vector magnetometer," Opt. Lett., vol. 44, no. 10, pp. 2494-2497, 2019.

[22] T. Erdogan, "Cladding-mode resonances in short- and long-period fiber grating filters," J. Opt. Soc. Am. A., vol. 14, no. 8, pp. 1760-1773, 1997.

[23] KS. Lee, T. Erdogan, "Fiber mode coupling in transmissive and reflective tilted fiber gratings," Appl. Opt., vol. 39, no. 9, pp. 1394-1404, 2000.

[24] KS. Lee, T. Erdogan, "Fiber mode conversion with tilted gratings in an optical fiber," J. Opt. Soc. Am. A., vol. 18, no. 5, pp. 1176-1185, 2001.

[25] G. Yin, S. Lou, Q. Li, and H. Zou, "Theory analysis of mode coupling in tilted long period fiber grating based on the full vector complex coupled mode theory," Opt. Laser Technol., vol. 48, no. 6, pp. 60-66, 2013.

[26] L. Dong, B. Ortega, and L. Reekie, "Coupling characteristics of cladding modes in tilted optical fiber Bragg gratings," Appl. Opt., vol. 37, no. 22, pp. 5099-5105, 1998.

[27] X. Chen et al., "In-Situ Detection of Small Biomolecule Interactions Using a Plasmonic Tilted Fiber Grating Sensor," J. Lightwave Technol., vol. 37, no. 11, pp. 2792-2799, 2019.

[28] D. Sun, T. Guo and B. Guan, "Label-Free Detection of DNA Hybridization Using a Reflective Microfiber Bragg Grating Biosensor with Self-Assembly Technique," J. Lightwave Technol., vol. 35, no. 16, pp. 3354-3359, 2017.

[29] L. Han, T. Guo et al., "Specific Detection of Aquaporin-2 Using Plasmonic Tilted Fiber Grating Sensors," J. Lightwave Technol., vol. 35, no. 16, pp. 3360-3365, 2016.

[30] Luo B, Wu S, Zou W, et al., "Label-free immunoassay for porcine circovirus type 2 based on excessively tilted fiber grating modified with staphylococcal protein A," Biosens. Bioelectron., vol.86, pp. 1054-1060, 2016.

[31] Luo B, Xu Y, Wu S, et al., "A novel immunosensor based on excessively tilted fiber grating coated with gold nanospheres improves the detection limit of Newcastle disease virus," Biosens. Bioelectron., vol.100, pp.169-175, 2017.

[32] Jiang B, Zhou K, Wang C, et al., "Label-free glucose biosensor based on enzymatic graphene oxide-functionalized tilted fiber grating," Sens. Actuators, B, vol.254, pp. 1033-1039, 2017.

[33] Jiang B, Bi Z, Hao Z, et al., "Graphene oxide-deposited tilted fiber grating for ultrafast humidity sensing and human breath monitoring," Sens. Actuators, B, vol. 293, pp. 336-341, 2019.

[34] Christophe Caucheteur*, Tuan Guo*, Fu Liu, Bai-Ou Guan, Jacques Albert*, "Ultrasensitive plasmonic sening in air using optical fibre spectral combs", Nature Communications., vol. 7, no. 13371, 2016.

[35] Y. Liu et al., "Plasmonic Fiber-Optic Photothermal Anemometers with Carbon Nanotube Coatings," J. Lightwave Technol., vol. 37, no. 13, pp. 3373-3380, 2019.

[36] Chiavaioli, F.; Gouveia, C.A.J. et al. "Towards a Uniform Metrological Assessment of Grating-Based Optical Fiber Sensors: From Refractometers to Biosensors," Biosensors., vol. 7, no. 23, 2017.

[37] T. Guo, F. Liu, B. Guan, and J. Albert, "Tilted fiber grating mechanical and biochemical sensors," Opt. Laser Technol., vol. 78, pp. 19–33, 2016.

[38] T. Erdogan. "Fiber Grating Spectra," J. Lightwave Technol., vol. 15, no. 8, pp. 1277-1294, 1997.